

## Perfect Softening of the Ferroelectric Mode in the Isotope-Exchanged Strontium Titanate of $\text{SrTi}^{18}\text{O}_3$ Studied by Light Scattering

M. Takesada,<sup>1,\*</sup> M. Itoh,<sup>2</sup> and T. Yagi<sup>3</sup>

<sup>1</sup>*Department of Physics, Hokkaido University, Sapporo 060-0810, Japan*

<sup>2</sup>*Materials and Structures Laboratory, Tokyo Institute of Technology, 4259 Nagatsuta, Yokohama 226-8503, Japan*

<sup>3</sup>*Research Institute for Electronic Science, Hokkaido University, Sapporo 060-0812, Japan*

(Received 21 February 2005; published 5 June 2006)

The  $E_u$  mode of the isotope-induced ferroelectric strontium titanate  $\text{SrTi}^{18}\text{O}_3$  shows a perfect softening at the ferroelectric phase transition temperature  $T_c$ , where the frequency of the underdamped mode approaches completely to zero within the instrumental resolution. The spectra of the Raman inactive soft  $E_u$  mode have been successfully observed owing to local symmetry breaking and by long-term accumulation of the spectral intensity with a high resolution technique. The mechanism of the phase transition is concluded to be an ideal displacive-type accompanied with perfect softening of the Slater-type polar  $E_u$  mode. The difference between the soft mode behavior of  $\text{SrTi}^{16}\text{O}_3$  and  $\text{SrTi}^{18}\text{O}_3$  indicates that the origin of the quantum paraelectric state of  $\text{SrTi}^{16}\text{O}_3$  lies in the quantum fluctuation of the oxide octahedron in the perovskite structure.

DOI: [10.1103/PhysRevLett.96.227602](https://doi.org/10.1103/PhysRevLett.96.227602)

PACS numbers: 77.84.Dy, 63.20.-e, 78.30.-j

The perovskite oxide strontium titanate  $\text{SrTiO}_3$  has been considered to belong to the typical quantum paraelectrics, because it keeps paraelectricity until  $T = 0$  K by the quantum fluctuation that might depress the occurrence of the ferroelectric order [1]. Indeed, at low temperatures below 4 K, the dielectric constant increases considerably but remains finite even near 0 K without any divergent behavior. The dynamics of the ferroelectric soft mode in the quantum paraelectrics also shows no freezing phenomenon, staying with the finite phonon frequency until 0 K according to the Lyddane-Sachs-Teller relationship [2,3]. Since the effect of quantum fluctuation was first suggested in Ref. [1], many intensive studies have been accumulated to elucidate the dynamics of the quantum fluctuation and also the soft mode behavior related to the quantum fluctuation in  $\text{SrTiO}_3$  and related materials. There are two types of soft modes in the low frequency region of  $\text{SrTiO}_3$ , as listed in the phonon correlation table [4]: the ferroelectric modes  $E_u$ ,  $A_{2u}$  [2–4] described above and the  $A_{1g}$ ,  $E_g$  modes related to the structural phase transition [5].

Recently, the ferroelectric phase transition in  $\text{SrTiO}_3$  was discovered at 23 K by exchange of  $^{16}\text{O}$  in  $\text{SrTiO}_3$  to its isotope  $^{18}\text{O}$  [6]. Since then, the phase transition mechanism of the isotope-exchanged strontium titanate  $\text{SrTi}^{18}\text{O}_3$  (hereafter abbreviated as STO18 and the ordinary one as STO16) has attracted the intense interest of many researchers in order to elucidate its phase transition mechanism related to the quantum fluctuations. The lowest energy phonon mode in STO18 has been searched for and analyzed to elucidate the soft mode dynamics near  $T_c$  by many authors [7–11]. However, any clear softening behavior has not been reported: By Raman scattering studies, the observation of the Raman inactive soft  $E_u$  mode has been tried, but the assignment of certain spectral feature to the  $E_u$  mode has not been convincing and unambiguous. Inelastic neu-

tron scattering has revealed the temperature dependence of the soft mode of STO18. It shows a small difference with the result reported on STO16 [11]. According to these experimental results about the low energy modes, theoretical and experimental works suggested a nondisplacive phase transition mechanism in STO18 [11,12]. However, quite recently the soft  $E_u$  mode observed in Ref. [11] was reassigned to be the  $A_{2u}$  mode [13]. The previous works give divergent conclusions due to the insufficient assignment of the soft  $E_u$  mode. In this situation we were strongly motivated to elucidate the soft mode dynamics of STO18 with an exact light scattering spectroscopy.

In the present Letter, we report a successful observation of the temperature dependence of the soft  $E_u$  mode in the extremely low frequency region using a high resolution technique and an ultrastable optical cryostat. The soft  $E_u$  mode demonstrates a perfect softening phenomenon. Here perfect softening means that the frequency of the mode approaches completely to zero value at  $T_c$  without any overdamping.

The polarized scattering light was analyzed by a Sandercock-type tandem Fabry-Perot interferometer on a six-pass stage with an averaged finesse more than 100 in typical free spectral ranges (FSR) of 3.3, 10.0 and  $16.7\text{ cm}^{-1}$ . The highest resolution is smaller than  $0.04\text{ cm}^{-1}$  in the FSR of  $3.3\text{ cm}^{-1}$ . To stabilize the experimental system, an Ar ion laser with a beam-lock system (Beamlok, SP) was used as a light source with longitudinal single mode at an average power of 100 mW and a wavelength of 514.5 nm. The analyzed light was detected by a photomultiplier (R464, Hamamatsu Photonics). The phonon wave vector  $q$  was selected to be parallel to the  $[001]_c$  axis of the cubic phase. The Raman spectra were observed in the scattering geometries VV, VH shown in the inset of Fig. 1, where V and H mean the polarization of light vertical and horizontal, respectively, to the  $(\bar{1}10)_c$  scattering

plane, and the former and latter symbols represent the incident and scattering light polarization, respectively. The sample is mounted in an optical cryostat (Optistat CF, Oxford) cooled by liquid helium. It was designed especially in order to keep the scattering position in the sample during the experiment. The temperature was stabilized within an error of  $\pm 0.01$  K. However, the observed value of temperature refers to the helium ambient to the sample in order to suppress strain by the contact with the temperature sensor, where we place the significance on the relative temperature of the sample from  $T_c$  rather than absolute values. The temperature in terms of absolute value thus includes experimental errors of about 0.5 K. The sample of a single crystal of STO18 was prepared with special high quality in a size of  $9 \parallel [001]_c \times 2 \parallel [\bar{1}10]_c \times 0.5 \parallel [110]_c$  to be favorable for a monodomain in the tetragonal phase [6]. The value of isotope concentration  $x$  in the sample studied was 95%.  $T_c$  is determined to be 25.9 K by the observation of the splitting of the  $E_g$  mode into  $A_2$  and  $B_1$  modes at the ferroelectric phase transition.

The Raman spectra of Fig. 1 in the VV geometry have been observed around  $T_c$ . The spectra show a drastic change near  $T_c$ . The longitudinal acoustic (LA) mode was observed at about  $0.7 \text{ cm}^{-1}$  as a pair of sharp peaks. Except for the LA mode, the spectra above  $T_c$  in Fig. 1 have two components below  $5 \text{ cm}^{-1}$  and around  $10\text{--}15 \text{ cm}^{-1}$  assigned to be the ferroelectric soft  $E_u$  mode and the  $A_{2u}$  mode, respectively. The intensity of soft  $E_u$  polar mode in Fig. 1 is extremely weak compared to the LA mode at around 30 K because of the Raman inactivity. With decreasing temperature, the spectrum of the  $E_u$  mode shifts to the central component critically and a drastic increase of

intensity with temperature approaching to  $T_c$ . The red points at 25.9 K in Fig. 1 are the spectrum at  $T_c$ .

The spectra from 29 K to  $T_c$  are well fitted as shown in Fig. 1 by susceptibility  $\chi_{E_u(\nu)}$ ,  $\chi_{A_{2u}(\nu)}$ , and  $\chi_{LA(\nu)}$  for the  $E_u$ ,  $A_{2u}$ , and LA modes, respectively,

$$I(\nu, T) \sim [n(\nu, T) + 1] \text{Im} \left( \sum_Q \chi_Q(\nu) \right), \quad (1)$$

$$\text{Im} \chi_Q(\nu) = \frac{\chi_Q(0) \nu_Q^2 \nu \frac{\gamma_Q}{2\pi}}{(\nu_Q^2 - \nu^2)^2 + \nu^2 \left( \frac{\gamma_Q}{2\pi} \right)^2},$$

where the sum runs over the three modes,  $Q = E_u, A_{2u}$ , and LA. The Bose factor  $n(\nu, T)$  is  $[\exp(h\nu/k_B T) - 1]^{-1}$ . The parameters  $\nu_Q$ ,  $\gamma_Q$  represent a frequency and a damping constant for the optical or acoustic mode, respectively. The frequencies  $\nu_{E_u}$ ,  $\nu_{A_{2u}}$  are plotted in Fig. 2. The  $E_u$  mode in Fig. 2 shows a critical and complete softening at  $T_c$  without any increase of damping. Above  $\sim 30$  K the spectra in Fig. 1 show the feature indicated by a broad ferroelectric microregion (FMR) response [14], which is not well fitted by Eq. (1). We will discuss elsewhere the relation between FMR and the  $E_u$  soft mode.

Below  $T_c$ , we have clearly observed the characteristic spectra with strong intensity in the frequency range below  $5 \text{ cm}^{-1}$ , as seen in Fig. 1. This shows that the soft mode becomes Raman active due to the symmetry change at  $T_c$ . The spectra near  $T_c$  are composed of three phonon modes except for the LA mode, since it is necessary for a well-fitting function to add another overdamped harmonic oscillator to the function of the paraelectric phase above  $T_c$ , as shown in the right inset in Fig. 1. With decreasing temperature, the lowest frequency phonon in Fig. 2 shows

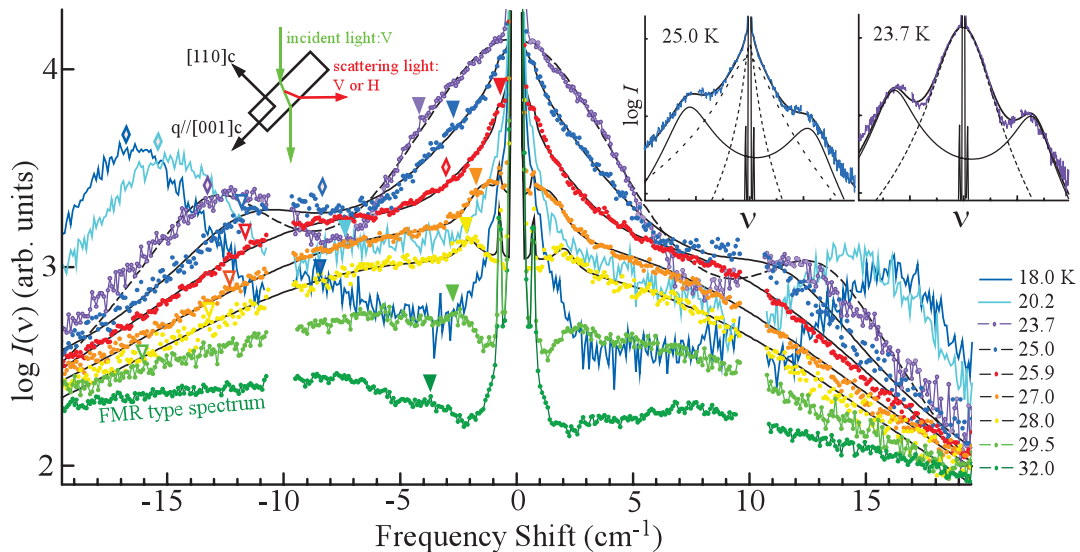


FIG. 1 (color). The low frequency Raman spectra with the VV geometry on FSR of  $10.0 \text{ cm}^{-1}$  in  $\text{SrTi}^{18}\text{O}_3$ . The black solid curves were determined by a least-squares fit. The lack of spectra around  $10.0 \text{ cm}^{-1}$  of FSR shows the experimental blind region for the tandem Fabry-Perot interferometer. The symbols represent the position of  $\nu_{E_u(A_1)}$  ( $\blacktriangledown$ ),  $\nu_{A_{2u}(B_1)}$  ( $\nabla$ ) and  $\nu_{B_2}$  ( $\blacklozenge$ ). The values of  $\nu_{B_2}$  and  $\nu_{A_{2u}}$  are much larger than the spectrum peak position due to the large  $\gamma$ . The left inset shows the scattering geometry. The right inset is a fitted result. The spectrum at 25.0 K includes two overdamped modes  $A_1(E_{u1})$  (inner dashed line),  $B_2(E_{u2})$  (outer dashed line), and two underdamped modes  $B_1(A_{2u})$  and LA (solid curves). One of the modes disappears at around 24 K.

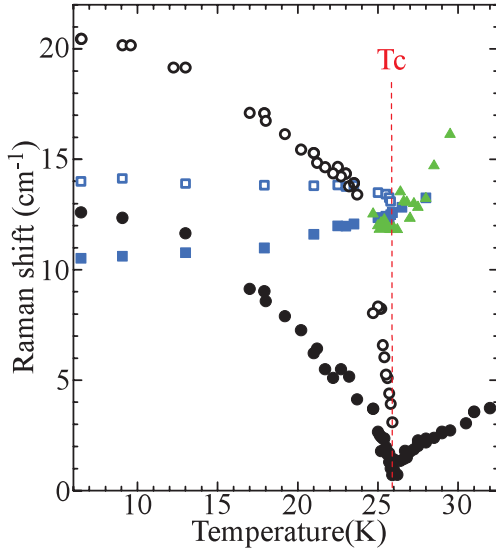


FIG. 2 (color). The temperature dependence of  $E_u$  (●),  $A_{2u}$  (▲), and  $E_g$  (■) modes above  $T_c$ , and  $A_1(E_{u1})$  (○),  $B_2(E_{u2})$  (○),  $B_1(E_{g1})$  (■),  $A_2(E_{g2})$  (□), and  $B_1(A_{2u})$  (▲) modes below  $T_c$  in  $\text{SrTi}^{18}\text{O}_3$ . The  $E_g$ ,  $B_1(E_{g1})$ , and  $A_2(E_{g2})$  modes are observed in the VH geometry (see Fig. 3).

continuous hardening below  $T_c$  from zero frequency. This mode is assigned to be the  $A_1(E_{u1})$  mode, where the symmetry in the parentheses indicates the one in the paraelectric phase. Both of the temperature dependences of the squared frequency of soft  $E_u$  and  $A_1(E_{u1})$  modes obey the Curie-Weiss law near  $T_c$ . The  $E_u$  and  $A_1$  modes in Fig. 2 show the soft mode behavior expected in a typical displacive-type mechanism of a ferroelectric phase transition. The present results are completely different from the previous ones observed above  $5 \text{ cm}^{-1}$  in STO18 [7–11]. The damping constant  $\gamma_{E_u}$  keeps a small value even just above  $T_c$ . Below  $T_c$ , the damping constant  $\gamma$  of the  $A_1$  mode shows a drastic increase with decreasing temperature and reaches a peak at about 2 degrees below  $T_c$ . The anomalous behavior of  $\gamma_{E_u}$  will be discussed below.

The temperature dependence of spectral intensity below  $5 \text{ cm}^{-1}$  in Fig. 1 shows a peak at about  $T_c - 2 \text{ K}$  different from  $T_c$ . The asymmetry of the spectra around zero frequency becomes remarkable with the temperature approaching to 0 K. The ratio of the observed intensity between Stokes and anti-Stokes spectra is well described by the Boltzmann factor. The  $A_{2u}$  mode in Fig. 2 softens with decreasing temperature above  $T_c$  and transforms continuously into the  $B_1(A_{2u})$  mode below  $T_c$ , though it is observed only near  $T_c$ . The  $B_1(A_{2u})$  mode is not expected to be observed from the selection rule. Such a behavior of the  $B_1(A_{2u})$  mode could be observed if the dynamic clusters with the structure above the  $T_c$  or with two (or more) polarization orientations exist in a narrow temperature range near the  $T_c$ . Disappearance of the  $B_1(A_{2u})$  mode with further cooling away from  $T_c$  seems to support this dynamical cluster model. Another different mode from  $A_1(E_{u1})$  shows hardening from zero frequency below  $T_c$

in Fig. 2. The mode is assigned as the  $B_2(E_{u2})$  mode. The temperature dependence of  $B_2(E_{u2})$  mode around 24 K in Fig. 2 shows an anomalous behavior, which might be recognized as an effect of mode coupling.

In VH geometry, the observed spectra below  $T_c$  in Fig. 3 are composed of five phonons including the LA mode. From the temperature dependence of phonon frequencies, they are assigned to be  $B_1(E_{g1})$ ,  $A_2(E_{g2})$ ,  $A_1(E_{u1})$ , and  $B_2(E_{u2})$  modes as denoted in Fig. 2. The  $B_1(E_{g1})$  and  $A_2(E_{g2})$  modes are consistent with previous works [8,9].

Here we have to consider the reason why the Raman inactive  $E_u$  mode is observed. The reason is discussed from the viewpoint of noncentrosymmetric clusters induced by defects in the crystal [14,15]. However, the structure of the cluster should not be restricted to the symmetry of the low temperature phase. The perovskite oxide crystals of STO18 and STO16 have defects caused, e.g., by oxygen vacancies. The local breakdown of crystal lattice symmetry occurs around the defects. The local symmetry breakdown region accompanied by a small lattice distortion might be extended to submicrometer scale region especially near  $T_c$ , because of the coupling with the critical ferroelectric fluctuation. From this viewpoint, the Raman inactive  $E_u$  mode can be observed reasonably. The observation of Raman scattering by inactive  $A_{2u}$  and  $E_u$  modes above  $T_c$  was reported in  $\text{SrTi}^{18}\text{O}_x^{16}\text{O}_{1-x}$  [15].

An anomalous behavior of the acoustic  $c_{44}$  mode has been reported around  $T_c$  by Brillouin scattering [8,16]; the drastic decrease of the value of frequency shift and the anomalous increase of intensity were presented. However, we have not observed such anomalous behavior in the  $c_{44}$  mode in the high quality STO18 samples of 95% and 96% concentrations in the present study. The difference indicates that the reported anomalous behavior of the  $c_{44}$  mode is not intrinsic for the transition, though it might be related to coupling effects induced by a sample-dependent internal stress created from the transition at 105 K [3] or FMR [14].

Finally, we discuss the anomalous behavior of the damping constant  $\gamma_{E_u}$  as follows:  $\gamma_{E_u}$  does not increase even

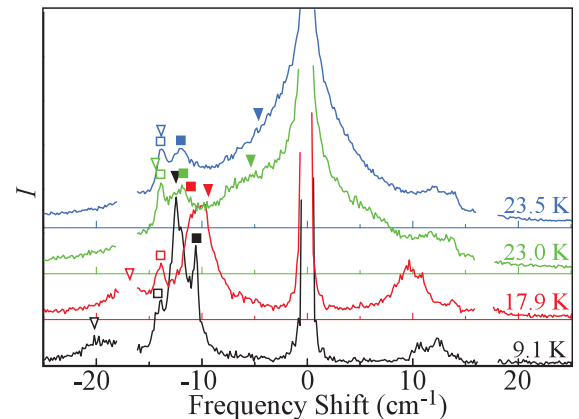


FIG. 3 (color). The Raman spectra with the VH geometry on FSR of  $16.7 \text{ cm}^{-1}$  in  $\text{SrTi}^{18}\text{O}_3$ . The symbols represent the  $B_1(E_{g1})$  (■),  $A_2(E_{g2})$  (□),  $A_1(E_{u1})$  (▼), and  $B_2(E_{u2})$  (▽) mode.

near  $T_c$  to keep the  $E_u$  mode in an underdamped state at  $T_c$ , in contrast to the case of an ordinary ferroelectric transition in the high temperature region where an extremely large value and/or anomalous increase of  $\gamma$  near  $T_c$  were reported in many cases, e.g., in  $\text{BaTiO}_3$  and  $\text{PbTiO}_3$  [17]. In the case of STO18, the ferroelectric transition takes place at the low temperature. A decrease of the number of thermally activated phonons suppresses the damping related to the mode coupling. However, an anomalous increase is still expected because of anharmonicity caused by the increase of the amplitude of the  $E_u$  mode upon approaching  $T_c$ . An adequate candidate for this mechanism which controls the behavior of  $\gamma_{E_u}$  is a new coherent phonon state of the  $E_u$  soft mode.

If the soft  $E_u$  mode takes a coherent state near  $T_c$ , the damping driven by a dephasing between each mode in the  $E_u$  phonon branch should be reduced, where the coherent phonon state could be related to a quantum coherence [18] on oxide octahedron in the perovskite structure. This can be a possible origin of the perfect softening of the ferroelectric  $E_u$  mode in STO18. Below  $T_c$ ,  $\gamma_{A_1}$  shows a drastic increase and a peak. These behaviors might be explained by the existence of dynamical clusters and a breakdown of the coherent phonon state just below the  $T_c$ , which disturbs the lattice vibrations associated with the soft phonons. However, there has been no report to establish the physical description for the origin of  $\gamma$  obtained from the spectroscopic analysis even in the typical ferroelectrics. More research is needed to elucidate conclusively the origin of the behavior of  $\gamma$  in STO18.

In the present Letter, the perfect softening of the ferroelectric soft  $E_u$  mode is found in the isotope-induced ferroelectric STO18. The mechanism of the ferroelectric phase transition in STO18 is concluded to be an ideal displacive-type associated to the Slater-type polar soft mode. Kozlov *et al.* have reported the ideal softening of the polar mode in the proper ferroelectric trisarcosine calcium chloride by the submillimeter monochromatic spectroscopy [19]. The present Letter is for the first time on a perfect softening of the Slater-type polar mode in the quantum ferroelectric STO18 [6]. If the transition is recognized as a second order one associated with the  $E_u$  soft mode, the structure of the ferroelectric phase is concluded to be orthorhombic,  $C_{2v}$ , with the polar axis along the  $[100]_c$  cubic direction according to theory based on the free energy function and the selection rules of the observed phonons, the  $A_1(E_{u1}), B_2(E_{u2})$  modes for the VV geometry and the  $A_1(E_{u1}), A_2(E_{g2}), B_1(E_{g1}), B_2(E_{u2})$  modes for VH. From the viewpoint of the difference of the soft phonon dynamics between STO18 and STO16, the quantum fluctuations of oxygen octahedra in perovskite-type crystals are considered to be at the origin of the quantum paraelectric state of STO16. Furthermore, the recently observed photoinduced cooperative phenomena with isotope effect might originate in the vibronic coupling between the soft phonon mode and excited electrons [20].

We are grateful to M. Tokunaga, Y. Noda, and S. Kinoshita for fruitful discussions. This work was partially supported by a Grant-in-Aid for Scientific Research (B) from JSPS No. 17340088 (M. T.) and a Grant-in-Aid for Scientific Research (S) from JSPS No. 17104004 (T. Y.).

\*Corresponding author.

Electronic address: mt@phys.sci.hokudai.ac.jp

- [1] K. A. Müller and H. Burkard, *Phys. Rev. B* **19**, 3593 (1979).
- [2] Y. Yamada and G. Shirane, *J. Phys. Soc. Jpn.* **26**, 396 (1969); K. Inoue, *Ferroelectrics* **52**, 253 (1983); P. A. Fleury and J. M. Worlock, *Phys. Rev.* **174**, 613 (1968).
- [3] H. Vogt, *Phys. Rev. B* **51**, 8046 (1995); A. Yamanaka, M. Kataoka, Y. Inaba, K. Inoue, B. Hehlen, and E. Courtens, *Europhys. Lett.* **50**, 688 (2000).
- [4] H. Uwe and T. Sakudo, *Phys. Rev. B* **13**, 271 (1976).
- [5] G. Shirane and Y. Yamada, *Phys. Rev.* **177**, 858 (1969).
- [6] M. Itoh, R. Wang, Y. Inaguma, T. Yamaguchi, Y.-J. Shan, and T. Nakamura, *Phys. Rev. Lett.* **82**, 3540 (1999); M. Itoh and R. Wang, *Appl. Phys. Lett.* **76**, 221 (2000).
- [7] K. Abe, K. Yamashita, Y. Tomita, T. Shigenari, R. Wang, and M. Itoh, *Ferroelectrics* **272**, 155 (2002).
- [8] H. Hasebe, Y. Tsujimi, R. Wang, M. Itoh, and T. Yagi, *Phys. Rev. B* **68**, 014109 (2003).
- [9] T. Shigenari, K. Abe, K. Yamashita, T. Takemoto, R. Wang, and M. Itoh, *Ferroelectrics* **285**, 41 (2003).
- [10] Y. Minaki, M. Kobayashi, Y. Tsujimi, and T. Yagi, *J. Korean Phys. Soc.* **42**, S1290 (2003).
- [11] Y. Yamada, N. Todoroki, and S. Miyashita, *Phys. Rev. B* **69**, 024103 (2004).
- [12] A. Bussmann-Holder and A. R. Bishop, *Phys. Rev. B* **70**, 024104 (2004); L. Zhang, W. Kleemann, J. Dec, R. Wang, and M. Itoh, *Eur. Phys. J. B* **28**, 163 (2002); R. Blinc, B. Zalar, A. Lebar, and M. Itoh, in *Fundamental Physics of Ferroelectrics 2003*, edited by P. K. Davies and D. J. Singh, AIP Conf. Proc. No. 677 (AIP, New York, 2003), p. 20.
- [13] Y. Noda, K. Mochizuki, H. Kimura, K. Kadoshita, Y. Kamata, M. Itoh, T. Kyomen, and R. Wang, *2004 Autumn Meeting of the Physical Society of Japan* (unpublished).
- [14] H. Uwe, K. B. Lyons, H. L. Carter, and P. A. Fleury, *Phys. Rev. B* **33**, 6436 (1986); W. Kleemann, A. Albertini, M. Kuss, and R. Lindner, *Ferroelectrics* **203**, 57 (1997).
- [15] H. Taniguchi, M. Takesada, M. Itoh, and T. Yagi, *J. Phys. Soc. Jpn.* **73**, 3262 (2004); M. Kasahara, R. Wang, M. Itoh, and T. Yagi, *J. Phys. Soc. Jpn.* **71**, 1254 (2002).
- [16] M. Yamaguchi, T. Yagi, R. Wang, and M. Itoh, *Phys. Rev. B* **63**, 172102 (2001).
- [17] M. E. Lines and A. M. Glass, *Principles and Applications of Ferroelectrics and Related Materials* (Oxford University, New York, 1977).
- [18] See, for example, A. J. Leggett, in *Material and Chance*, edited by J. Souletie, J. Vannimenus, and R. Stora (Elsevier, New York, 1987), p. 395.
- [19] G. V. Kozlov, A. A. Volkov, J. F. Scott, G. E. Feldkamp, and J. Petzelt, *Phys. Rev. B* **28**, 255 (1983).
- [20] M. Takesada, T. Yagi, M. Itoh, and S. Koshihara, *J. Phys. Soc. Jpn.* **72**, 37 (2003).